Physica Scripta

PAPER

Shannon entropy of a particle on a conical surface

L M Arvizu, E Castaño and N Aquino*

Departamento de Física, Universidad Autónoma Metropolitana-Iztapalapa, Av. Ferrocarril San Rafael Atlixco 186, Iztapalapa, C. P. 09310, Ciudad de México, Mexico

* Author to whom any correspondence should be addressed.

E-mail: arvizu13@xanum.uam.mx, ele@xanum.uam.mx and naa@xanum.uam.mx

Keywords: Shannon entropy, particle on a cone surface, energy eigenvalues, radial standard deviation

OPEN ACCESS

RECEIVED
8 May 2024

REVISED
2 August 2024

ACCEPTED FOR PUBLICATION
15 August 2024

PUBLISHED
29 August 2024

Abstract

In this work we solve the time-independent Schrödinger equation of a particle restricted to move on the surface of a circular cone of finite height. The energy eigenvalues, as well as the corresponding wave functions, are obtained analytically as a function of, r and ϕ, the radial distance to the apex, $0 \leqslant r \leqslant r_0$, and the angular variable around the axis of the cone. We compute the Shannon entropy of this system in both configuration and momentum space as a function of r_0 and θ_0, the angular semi-aperture of the cone. In configuration space, the Shannon entropy decreases, signalling a more pronounced localization, as either r_0 or θ_0 diminish; in momentum space, an opposite behaviour happens, i.e., the Shannon entropy increases when either, r_0 or θ_0, decrease. We also compute the radial standard deviation; we find that the Shannon entropy better describes the localization-delocalization phenomena. The present results agree with those previously published for a particle confined to a circle of radius r_0, which corresponds to $\theta_0 = \pi/2$ in the present case.

1. Introduction

Spatially confined quantum systems have gained much interest in recent years since one can effectively design their electronic properties by modifying the energy quantization, something that is achived by changing their size, shape and dimensionality, as well as by using different materials and applying external fields. Recently, different experimental techniques have been developed for the elaboration of a variety of confined quantum systems that comprehends quantum wells, wires and dots, electronic structure of atoms and molecules subjected to external high pressures, specific heat of monocrystals under high pressures, atoms trapped in cavities, and nanopores, [1–18], among many others. Recent progress on the field of confined atoms and molecules can be reviewed in [19].

In recent years, a great deal of work has been devoted to the experimental and theoretical study of quantum dots of different shapes that include spherical, ellipsoidal, cylindrical, conical, pyramidal and lenticule geometries, [20–25], since theses systems have a wide range of applications in electronic and optoelectronic technology, [26, 27].

Quantum mechanics of particles inside cones has also been shown to be a fruitful model for studying the effects of spatial quantization, [28–30], and Gravesen *et al* studied states of a particle on a surface of revolution forming a truncated cone [31].

Information measures such as Shannon entropy, Fisher information, disequilibrium, Tsallis and Renyi entropies, among others, have been successfully used in different works that include the derivation of fundamental equations of physics, image retrieval and indexing, machine learning, seismology, biological imaging, cryptography, noise theory, black holes and atoms [32–59]. Particular emphasis has been placed in the study of Shannon entropy in free atoms and molecules [41–45]. Recently, it has been used in the study of hydrogen and helium atoms as well as in many electron atoms confined in penetrable and impenetrable cavities [48–58].

A commonly used measure of the uncertainty of the position of a particle in one dimension is the standard deviation. When the standard deviation is small the particle will be localized, while when the standard deviation

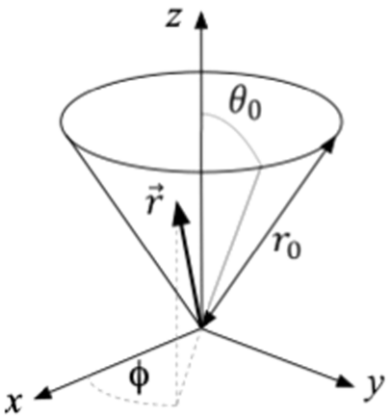

Figure 1. A particle on the cone surface.

is large the particle will be delocalized. In the theoretic information there are few measures that can be used as measures of localization-delocalization, some of them are Shannon entropy [46–57], Fisher information [47, 49, 54, 56, 57] and disequilibrium [54]. Shannon entropy is a global measure of the spread of the probability density $\rho(r)$. The Fisher information is a measure of the narrowness or concentration of electron density $\rho(r)$, it is local measure. The disequilibrium gives a measure of the probability density $\rho(r)$ respect to the equiprobability.

In this work, we study a particular quantum dot model: a single free electron that moves on the surface of a circular cone whose semi-angular aperture, θ_0, can be varied at will; please see figure 1. Then, when $\theta_0 = \pi/2$ we have a flat system, and as θ_0 is decreased we obtain a needel like structure, but always having two-dimensional system that leads to analytical expressions for the proper energies and eigenfunctions, a symplifying feature that allows the study of quantum information properties in an accurate manner.

Our particular proposal is part of more general one which includes the study of so-called *atoms a la mode*, artificial atoms, where one can design its properties by varying size and shape, effective mass, as well as the use of applied external fields in ways that enhance energy quantization to obtain system with novel properties.

This work is organized as follows: in section 2 we obtain and solve the Schrödinger equation for a particle confined on the surface cone in curvilinear coordinates. In section 3 we give the theoretical framework for the Shannon entropy in configuration and momentum space. The radial standard deviation is presented in section 4. In section 5 we discuss our results. Finally, in section 6 we give our conclusions.

2. Schrödinger equation in curvilinear coordinates

Consider a particle of mass m_0 is moving on the surface of a circular cone, the geometry is shown in figure 1. The origin of the coordinate system is placed at the apex of the cone, the cone symmetry axis is the z axis and, θ_0 is the semi-angular aperture of the cone. The motion of the particle is restricted to the cone surface, hence its position is completely described by two degrees of freedom. We use the following curvilinear coordinates

$$u^1 = r, \;\; u^2 = \phi, \tag{1}$$

where r is the distant from the origin to a point on the cone surface, and ϕ is the azimuthal angle.

In this coordinates, the position vector is given by

$$\vec{r} = r\hat{r}, \tag{2}$$

where $\hat{r}$ is the radial unit vector

$$\hat{r} = \sin\theta_0 \cos\phi\hat{x} + \sin\theta_0 \sin\phi\hat{y} + \cos\theta_0\hat{z}, \tag{3}$$

and, therefore

$$\overrightarrow{dr} = dr\hat{r} + r \sin\theta_0 d\phi\hat{\phi}. \tag{4}$$

In general, the square of the differential element of arc on the surface, using the Einstein sum convention, is given by [60, 61]

$$ds^2 = \overrightarrow{dr} \cdot \overrightarrow{dr} = g_{ij}du^i du^j, \tag{5}$$

where g_{ij} are the components of the metric tensor, and $(g^{ij}) = (g_{ij})^{-1}$. Let $g = det\,(g_{ij})$, which in our case is then

$$g = r^2 \sin^2\theta_0. \tag{6}$$

The kinetic energy operator is as follows

$$\begin{aligned} T &= -\frac{\hbar^2}{2m_0}\left[\frac{1}{\sqrt{g}}\frac{\partial}{\partial u^i}\left(\sqrt{g}\; g^{ij}\frac{\partial}{\partial u^j}\right)\right] \\ &= -\frac{\hbar^2}{2m_0}\left(\frac{1}{r}\frac{\partial}{\partial r}\left(r\frac{\partial}{\partial r}\right) + \frac{1}{r^2\sin^2\theta_0}\frac{\partial^2}{\partial\phi^2}\right). \end{aligned} \tag{7}$$

The differential element of area is given by

$$dA = \sqrt{g}du^1du^2 = r\,\sin\,\theta_0 dr\; d\phi. \tag{8}$$

We are interested in the motion of an electron ($m_0 = m_e$) on an impenetrable cone of finite size. Then, the Hamiltonian in atomic units ($\hbar = m_e = e = 1$) is given by

$$H = -\frac{1}{2}\left(\frac{1}{r}\frac{\partial}{\partial r}\left(r\frac{\partial}{\partial r}\right) + \frac{1}{r^2\sin^2\theta_0}\frac{\partial^2}{\partial\phi^2}\right) + V(r), \tag{9}$$

where

$$V(r) = \begin{cases} 0, & r < r_0 \\ \infty, & r > r_0 \end{cases}. \tag{10}$$

The Schrödinger equation in the region $r < r_0$ is given by

$$-\frac{1}{2}\left(\frac{1}{r}\frac{\partial}{\partial r}\left(r\frac{\partial}{\partial r}\right) + \frac{1}{r^2\sin^2\theta_0}\frac{\partial^2}{\partial\phi^2}\right)\psi(r,\,\phi) = E\psi(r,\,\phi), \tag{11}$$

for $r > r_0$, the wave function is zero. The problem is symmetric around the z axis, henceforth the solution of the Schrödinger equation can writen as follows:

$$\psi(r,\,\phi) = R(r)\frac{e^{im\phi}}{\sqrt{2\pi}},\;\; |m| = 0,\,1,\,2,\,3,\ldots \tag{12}$$

Substituting equation (12) in equation (11) we obtain the following differential equation for $R(r)$, the radial wave function:

$$\frac{d^2R}{dr^2} + \frac{1}{r}\frac{dR}{dr} - \frac{\mu^2}{r^2}R = -2ER, \tag{13}$$

where

$$\mu \equiv \frac{|m|}{\sin\,\theta_0},\;\; \theta_0 \neq 0. \tag{14}$$

In order to solve (13) we make a change of variable,

$$z \equiv kr, \tag{15}$$

with

$$k = \sqrt{2E}. \tag{16}$$

Substituting equation (15) in equation (13) we get

$$z^2\frac{d^2R}{dz^2} + z\frac{dR}{dz} + (z^2 - \mu^2)R = 0, \tag{17}$$

which is the Bessel differential equation, whose general solution is

$$R(z) = AJ_\mu(z) + BJ_{-\mu}(z). \tag{18}$$

Applying the boundary condition $R(z = z_0) = 0$, and considering that $R(z)$ must be finite at the origin, it follows that $B = 0$, and, therefore

$$R_{n,m}(r) = AJ_\mu\left(\chi_{n,\mu}\frac{r}{r_0}\right), \tag{19}$$

where J_μ is the Bessel function of first kind [62] and order μ, and $\chi_{n,\mu}$ is the n*th* zero of J_μ. The normalization constant is given by:

$$A = \left[\frac{2}{r_0^2 \sin\theta_0 \, J_{\mu+1}^2(\chi_{\mu,n})} \right]^{1/2}. \tag{20}$$

Therefore, the normalized eigenfunctions of equation (11) are given by

$$\psi_{n,m}(r, \phi) = R_{n,m}(r) \frac{e^{im\phi}}{\sqrt{2\pi}},$$

$$n = 1, 2, 3,\ldots, |m| = 0, 1, 2, 3,\ldots$$

being their respective energy eigenvalues:

$$E_{n,m} = \frac{\hbar^2 {\chi_{\mu,n}}^2}{2m_0 {r_0}^2}. \tag{21}$$

For $m \neq 0$, $E_{n,-m} = E_{n,m}$, since μ has the same value for m and $-m$, according to equation (14).

The wave functions in momentum space are obtained by the Fourier transform of $\psi_{n,m}(r, \phi)$, as follows:

$$\Phi_{n,m}(p, \vartheta) = \frac{1}{2\pi} \int_{r=0}^{r_0} \int_{\phi=0}^{2\pi} \psi_{n,m}(r, \phi) e^{-i\vec{p}\cdot\vec{r}} \sin\theta_0 r dr d\phi, \tag{22}$$

where

$$\vec{p} \cdot \vec{r} = pr \cos(\vartheta - \phi),$$

we obtain

$$\Phi_{n,m}(p, \vartheta) = \frac{i^m e^{im\vartheta}}{\sqrt{2\pi}} \int_0^{r_0} R_{n,m}(r) J_m(pr) \sin\theta_0 r \, dr. \tag{23}$$

3. Shannon entropy

In this section we compute the Shannon entropy for different states as a function of r_0 and θ_0. It is worth noticing that Shannon entropy is a functional of the probability density that a measures the dispersion of this quantity.

In configuration space the probability density ρ is given by

$$\rho_{n,m}(r, \phi) = |\psi_{n,m}(r, \phi)|^2. \tag{24}$$

Whereas in momentum space

$$\gamma_{n,m}(p, \vartheta) = |\Phi_{n,m}(p, \vartheta)|^2. \tag{25}$$

3.1. Shannon entropy in configuration space

The Shannon entropy S_r in configuration space is given by

$$S_r(n, m) = -\int_{r=0}^{r_0} \int_{\phi=0}^{2\pi} \rho_{n,m}(r, \phi) ln(\rho_{n,m}(r, \phi)) \sin\theta_0 r \, dr \, d\phi. \tag{26}$$

We should note that the probability density $\rho_{n,m}(r, \phi)$ is normalized to unity.

3.2. Shannon entropy in momentum space

The Shannon entropy in momentum space is given by

$$S_p(n, m) = -\int_{p=0}^{\infty} \int_{\theta=0}^{2\pi} \gamma_{n,m}(p, \vartheta) ln(\gamma_{n,m}(p, \vartheta)) \frac{p}{\sin\theta_0} dp \, d\vartheta, \tag{27}$$

where $\gamma_{n,m}(p, \vartheta)$ is given by equation (25), and is also normalized to unity. The interpretation of S_p and S_r are similar to each other in their respective spaces.

3.3. Entropic sum

Balinicki-Birula and Mycielski (BBM) [63] showed that the total Shannon entropy S_t satisfies the following uncertainty principle

$$S_t = S_r + S_p \geqslant D(1 + \ln\pi), \tag{28}$$

where D is the dimensionality of the system.

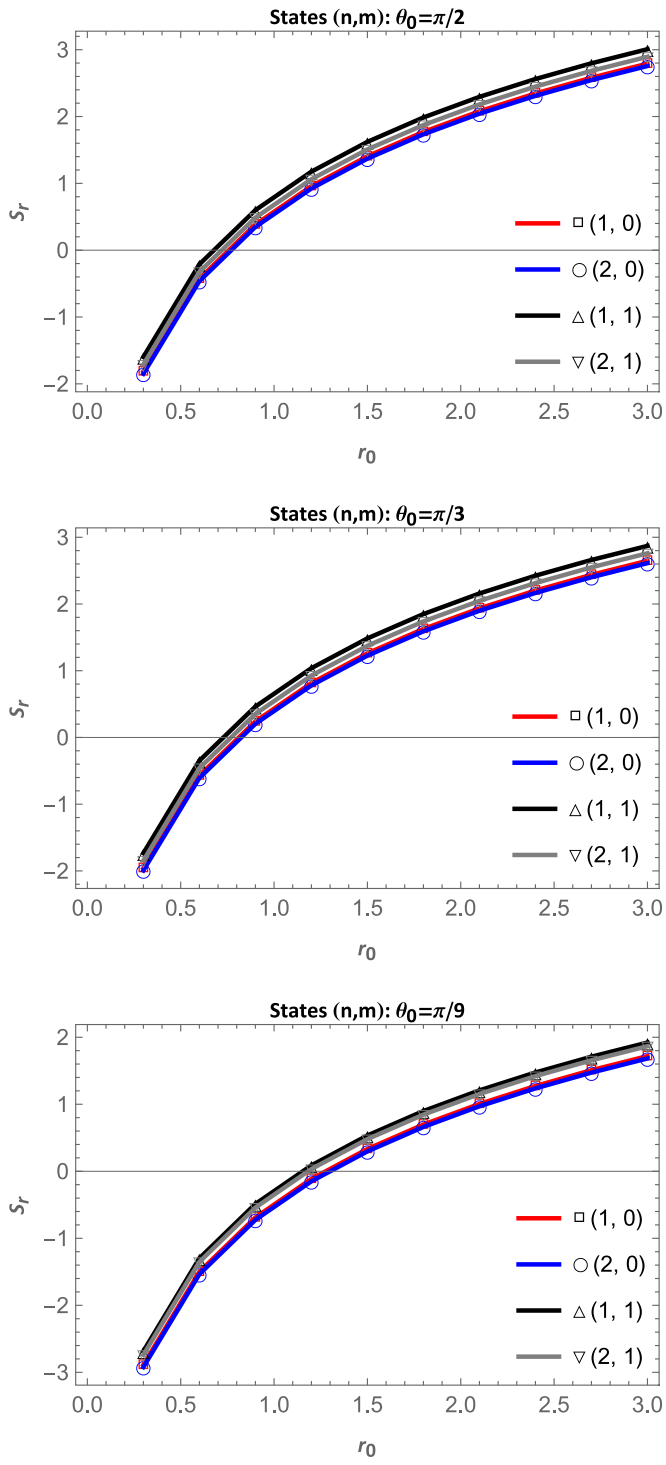

Figure 2. Shannon entropy as a function of the confining radius for $\theta_0 = \pi/2,\ \pi/3,\ \pi/9$.

4. The radial standard deviation

The radial standard deviation has been used as a measure of localization in the quantum corral [51] and in the problem of the motion of a particle in a circle in the presence of a constant magnetic field [53].

The radial density is defined by integrating the probability density with respect to angle ϕ as follows:

$$\rho_r(r) = \int_0^{2\pi} |\psi_{n,m}(r,\ \phi)|^2 d\phi. \tag{29}$$

The radial probability distribution $\rho_r(r)rdr$ represent the probability of finding the particle between the radial distances r and $r + dr$. The radial standard deviation σ_r is given in therms of the radial density

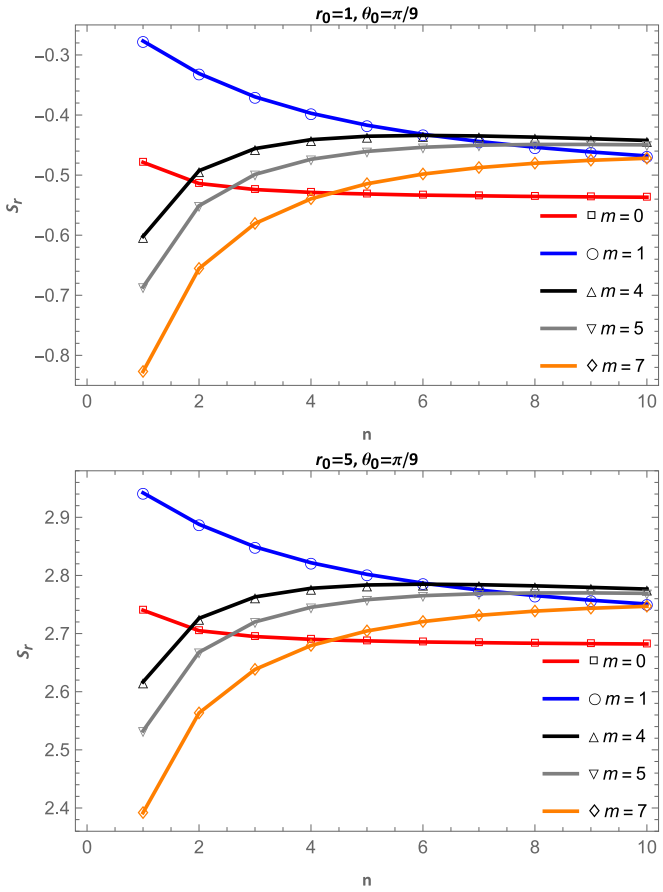

Figure 3. Shannon entropy as a function of n for two different values of confining radius $r_0 = 1$ and 5 for a fixed value of the apex angle $\theta_0 = \pi/9$, and angular quantum number $m = 0,\ 1,\ 4,\ 5$ and 7 as noted.

$$\sigma_r = \left[\int_0^{r_0} r^2 \rho_r(r) r dr - \left(\int_0^{r_0} r \rho_r(r) r dr\right)^2\right]^{1/2}. \tag{30}$$

The radial standard deviation is associated with the dispersion of the radial density. This quantity is used as a measure of particle localization-delocalization since when σ_r is very small, the probability density is sparsely scattered and the particle is more localized, while when σ_r is very large, the probability density is highly scattered and the particle is delocalized.

5. Results

5.1. Shannon entropy in configuration space

In figure 2 we show the Shannon entropy values for few states as a function of the confining radius r_0, for selected values of the apex angle, $\theta_0 = \pi/2,\ \pi/3$ and $\pi/9$; the states are labeled as $(n,\ m)$ where n is the radial quantum number and m is the angular quantum number.

The Shannon entropy for all the states diminishes (localization increases) as the confining radius r_0 decreases, since the surface available for the motion of the electron gets reduced with r_0. The Shannon entropy curves for $\theta_0 = \pi/2,\ \pi/3$ are almost identical to each other. Noticed that for a fixed value of r_0 the Shannon entropy decreases (localization increases) as the apex angle is reduced. For $\theta_0 = \pi/2,\ \pi/3$, the decrease in Shannon entropy values is very slight but for $\theta_0 = \pi/9$ it is more pronounced. The present results for $\theta_0 = \pi/2$ are in full agreement with those previously published in the literature [51–53]. When the spatial confinement increases, the area in which the electron moves is reduced, the Shannon entropy decreases (localization) and even its value can become negative, this is a typical behavior of the Shannon entropy in confined systems [46–57].

In figure 3 we show the Shannon entropy as a function of quantum number n for two different values of the confining radius $r_0 = 1$ and 5, and $\theta_0 = \pi/9$.

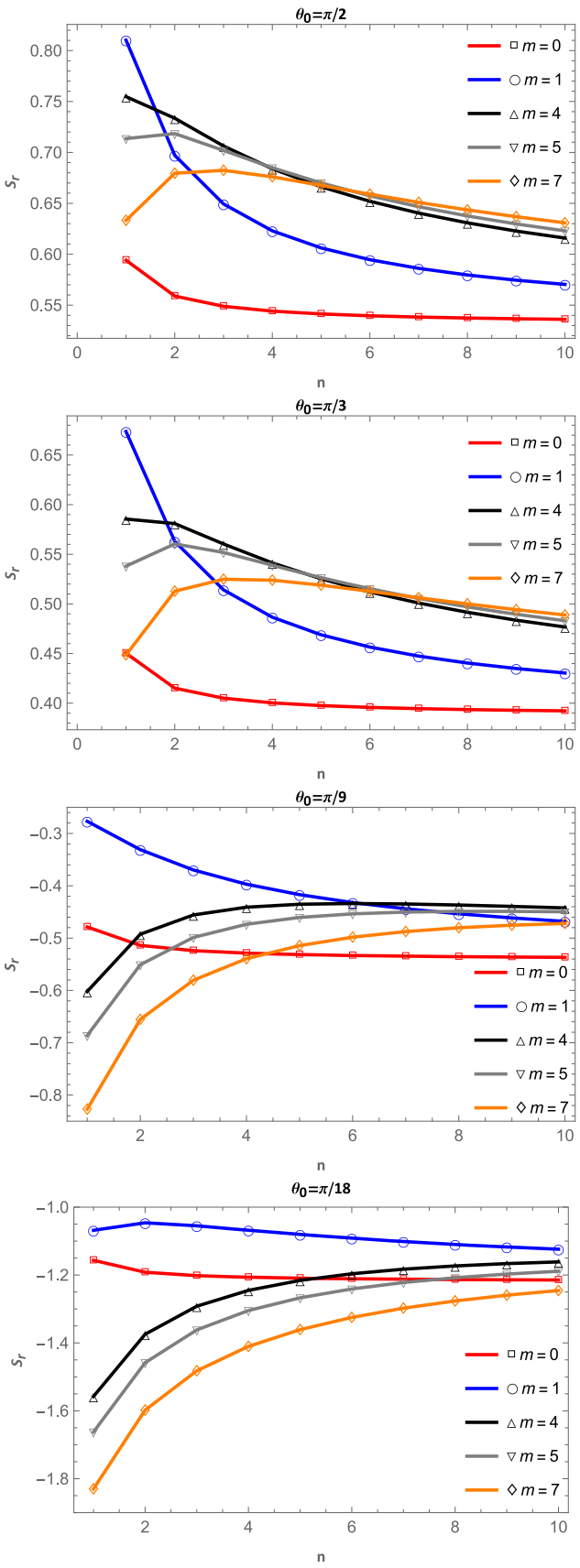

Figure 4. The Shannon entropy as a function of the radial quantum number n for four different apex angles $\theta_0 = \pi/2,\ \pi/3,\ \pi/9$ and $\pi/18$; $r_0 = 1$, and angular quantum number $m = 0,\ 1,\ 4,\ 5$ and 7 as noted.

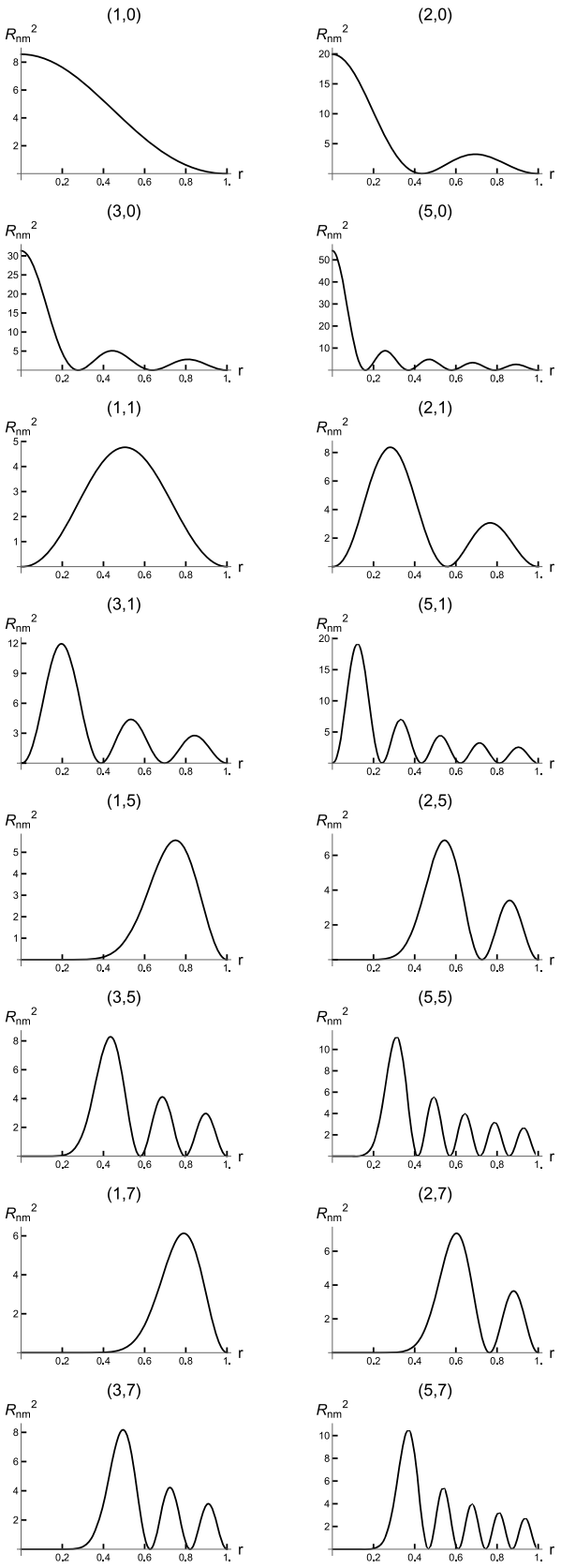

Figure 5. Probability density $R^2_{n,m}$ for different states (n, m) for $\theta_0 = \pi/3$.

The Shannon entropy curves for both confining radii are identical in shape, except for a translation in the direction of the vertical axis. For this reason, we can use any value of r_0 to study the behavior of the Shannon entropy in configuration space; hereafter we will use $r_0 = 1$.

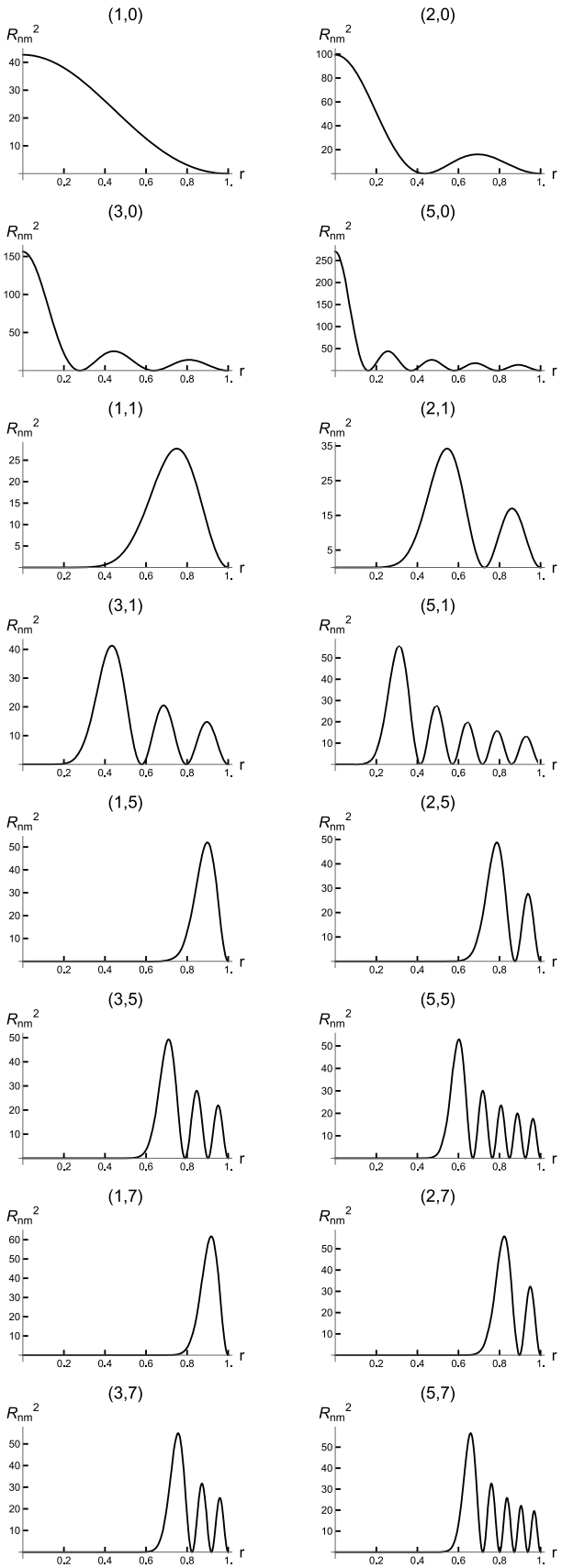

Figure 6. Probability density $R^2_{n,m}$ for different states (n, m) for $\theta_0 = \pi/18$.

In figure 4 we show the Shannon entropy as a function of the quantum number n for a fixed radius $r_0 = 1$ and four different values of the apex angle $\theta_0 = \pi/2,\ \pi/3,\ \pi/9$ and $\pi/18$ and several quantum angular numbers.

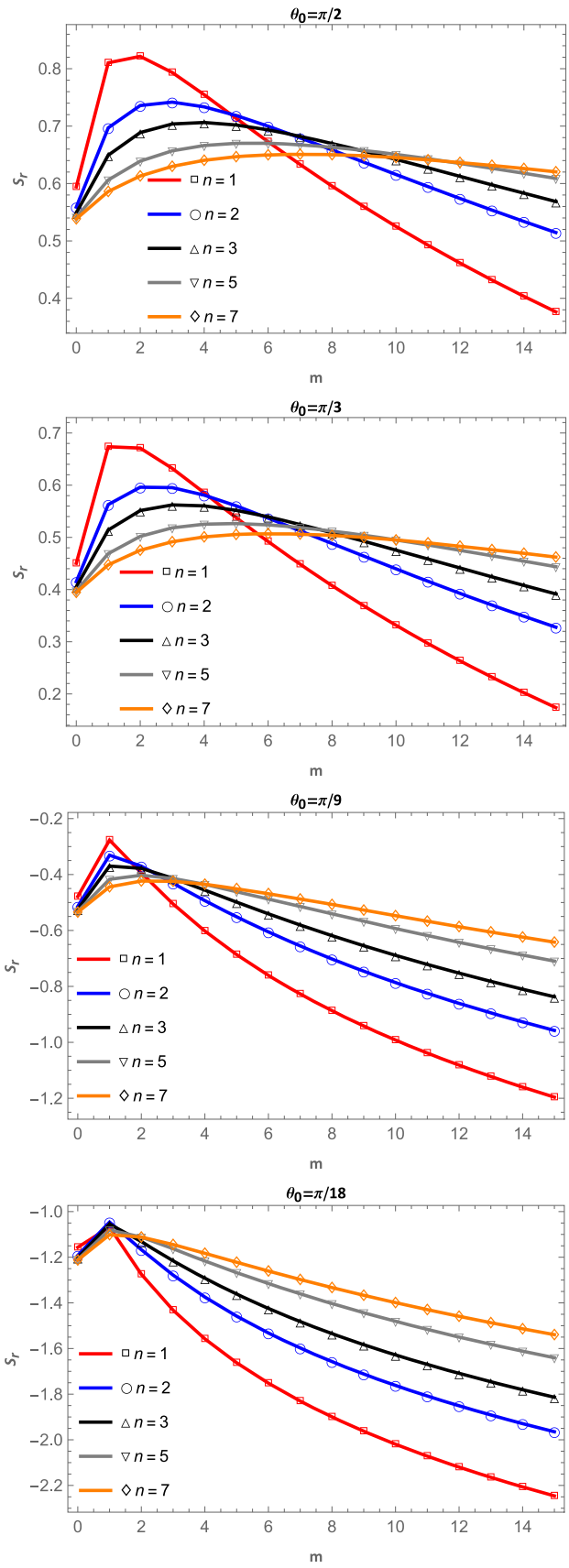

Figure 7. Shannon entropy as a function of the angular quantum number m for four different apex angles $\theta_0 = \pi/2,\ \pi/3,\ \pi/9$ and $\pi/18$ and for a value of $r_0 = 1$.

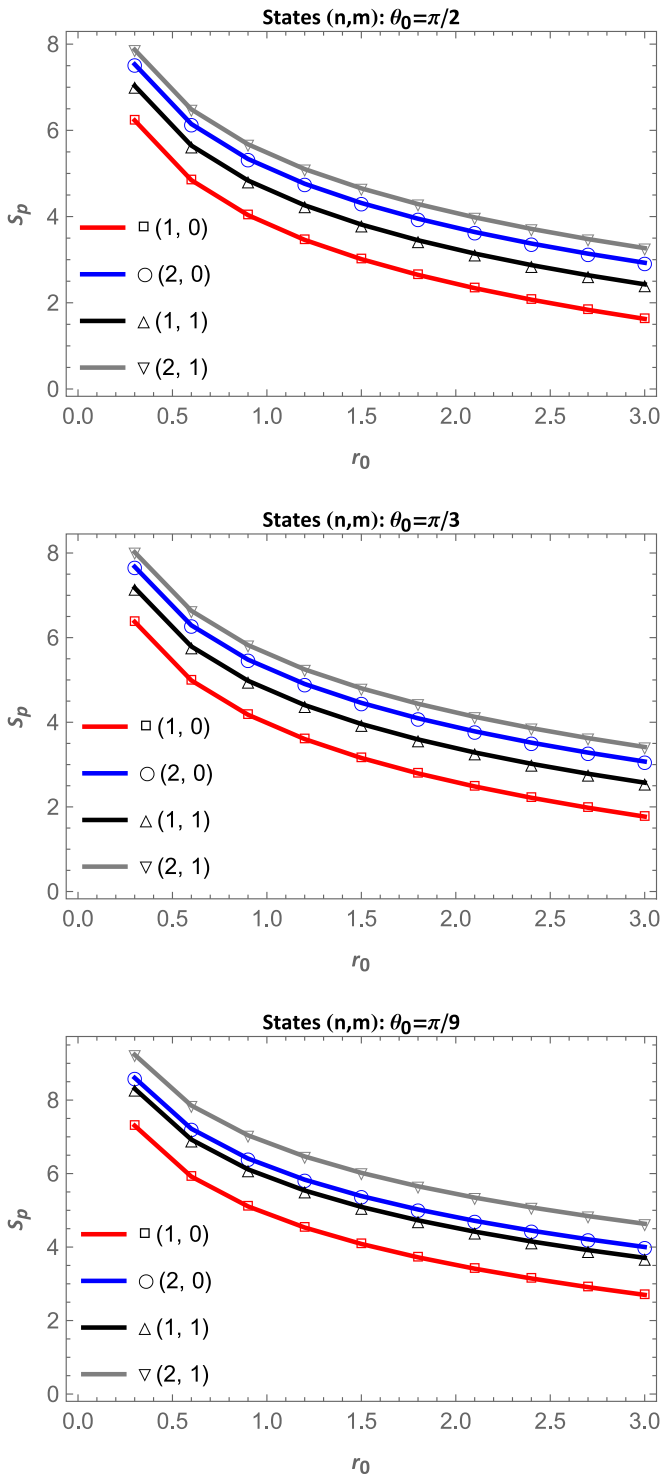

Figure 8. Shannon entropy as a function of the confining radius r_0 for $\theta_0 = \pi/2,\ \pi/3,\ \pi/9$.

For $\theta_0 = \pi/2$, our results are in complete agreement with the figure 2 obtained by [51], as expected. The Shannon entropy curves for $m = 0$–4 diminish (localization) as the radial quantum number n grows, while for $m > 4$, S_r increases (delocalization) until it reaches a maximum value and then decreases, this behavior in the Shannon entropy was explained by Corzo *et al* [42] by using the plot of the $R^2_{n,m}(r)$.

Also notice that the results for Shannon entropy shown in figure 4 for $\theta_0 = \pi/2$ and $\theta_0 = \pi/3$ are very similar among them. The lower Shannon entropy values (localization) for $\theta_0 = \pi/2$ are obtained for the states (10,0) and (10,1), as can be seen from figure 4. The same conclusion applies for $\theta_0 = \pi/3$.

The behavior of the Shannon entropy is understood using figure 5, where $R^2_{n,m}(r)$ is shown for few states. The S_r for states with $m = 5$ and $m = 7$ first increases (delocalize), reach a maximum value and begins to

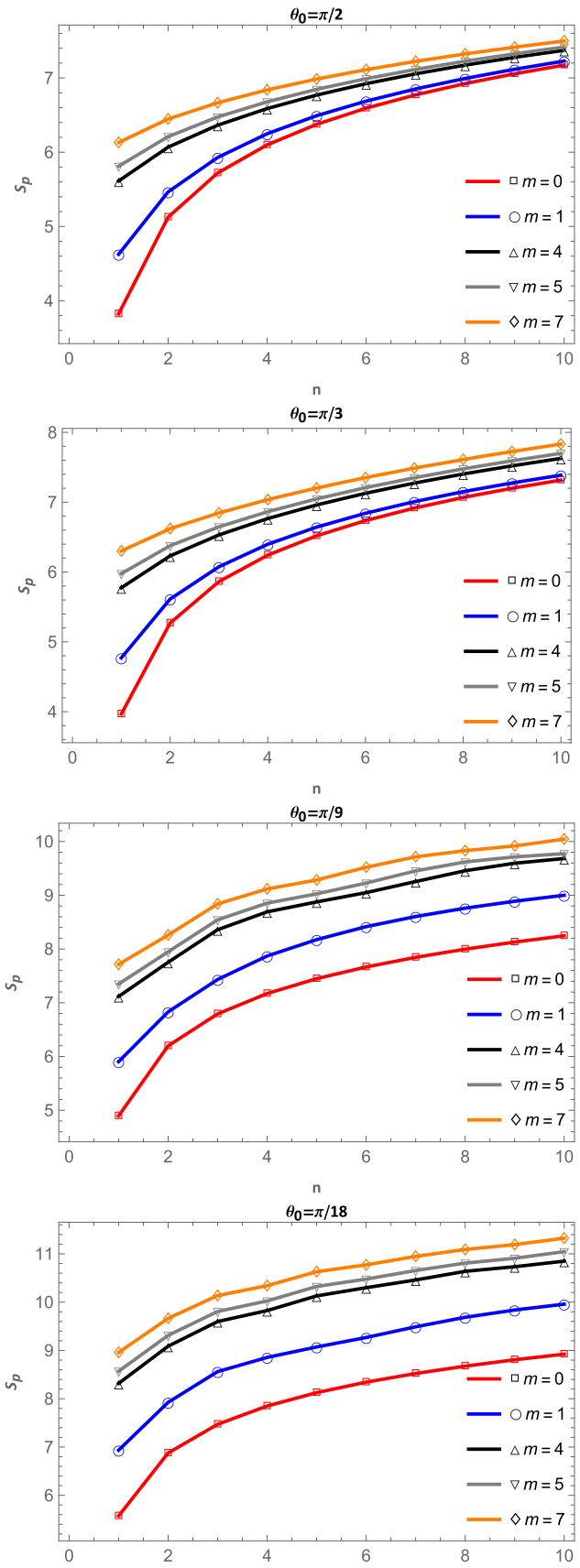

Figure 9. Shannon entropy in momentum space as a function of the quantum number n for a fixed value r_0.

decrease as n increases. From figure 5 it can be seen that state $(1, 5)$ is more localized than $(2, 5)$ and the latter is less localized than $(3, 5)$, so $S_r\ (1,\ 5) < S_r\ (2,\ 5)$ and $S_r\ (2,\ 5) < S_r\ (3,\ 5)$. The explanation for the Shannon entropy for the curve with $m = 7$, is analogous.

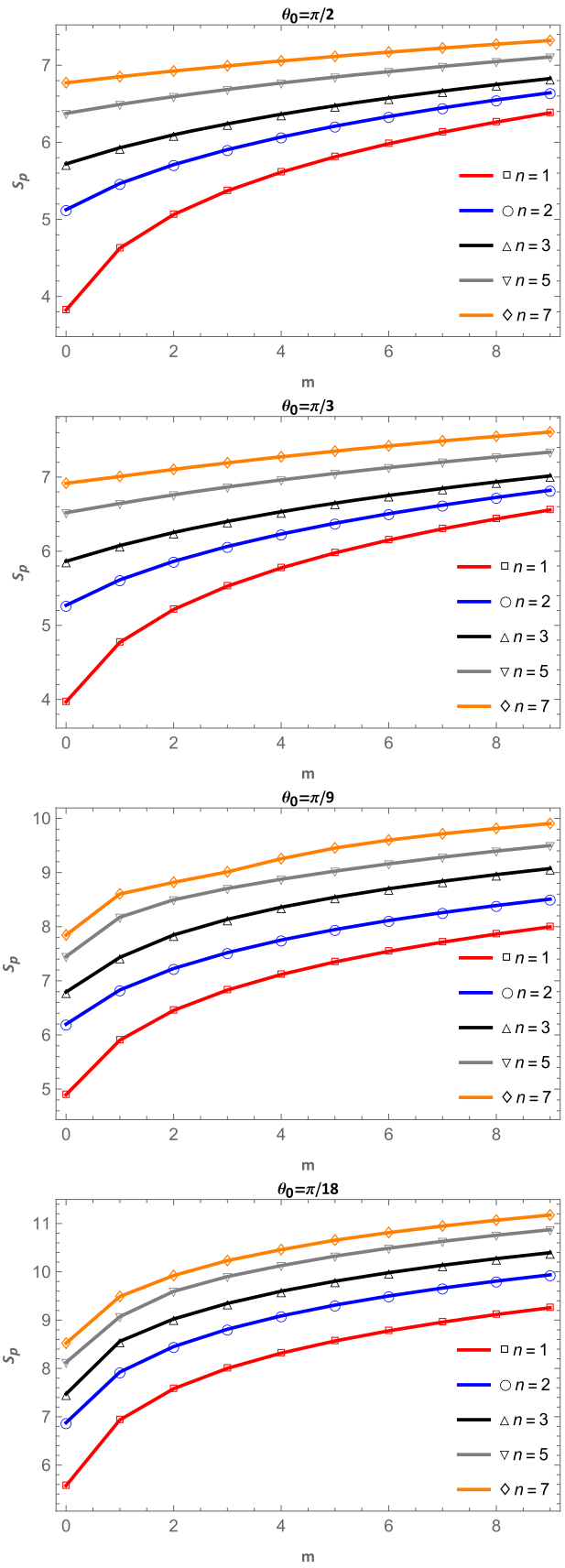

Figure 10. Shannon entropy in momentum space as a function of the quantum number m for $r_0 = 1$.

From the results $\theta_0 = \pi/9$ and $\pi/18$ it is observed that as the θ_0 decreases, the Shannon entropy also decreases, indicating an increased localization. The difference in entropies $S_r\ (n,\ 1) - S_r\ (n,\ 0)$ becomes smaller as n increases. The Shannon entropy for states with $m > 4$ starts to grow as n increases in the range

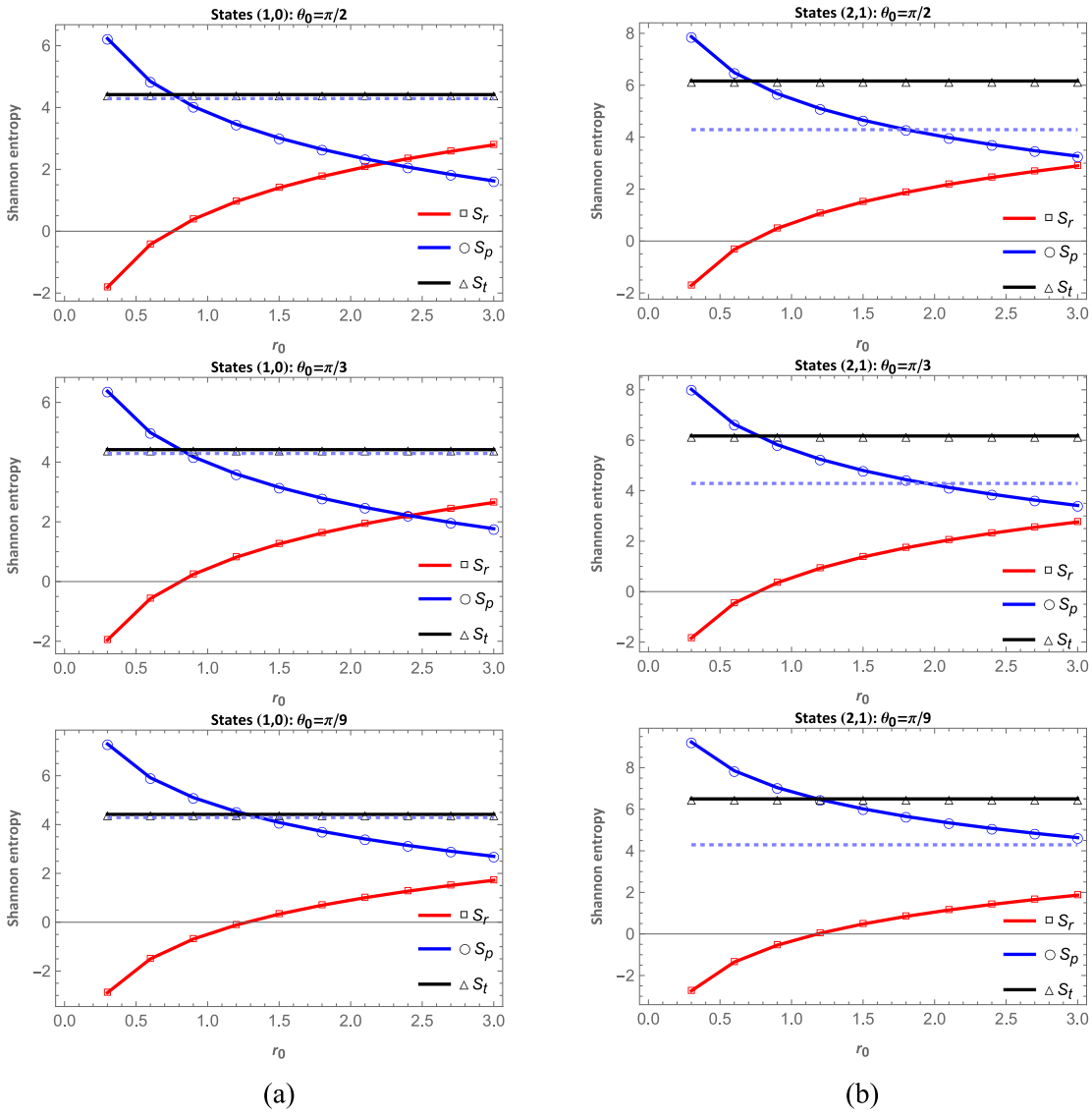

Figure 11. (a) Entropic sum as a function of r_0 for the state (1,0), for different values of the apex angle θ_0. The dotted line corresponds to the value of the bound of the BBM uncertainty principle; $S_t = S_r + S_p \geqslant 2(1 + \ln \pi) = 4.2896$, as expected. (b). Entropic sum as a function of r_0 for the state (2,1), for different values of the apex angle θ_0. The dotted line corresponds to the value of the bound of the BBM uncertainty principle; $S_t = S_r + S_p \geqslant 2(1 + \ln \pi) = 4.2896$, as expected.

$1 \leqslant n \leqslant 10$. The behavior of S_r as a function of n can be understood by analyzing figure 6, where $R^2_{n,m}(r)$ is shown for several (n, m) states.

Figure 7 shows the behavior of Shannon entropy as a function of quantum number m for four different angle $\theta_0 = \pi/2,\ \pi/3,\ \pi/9$ and $\pi/18$ and $r_0 = 1$.

Our results are in full agreement with those of [53] for $\theta_0 = \pi/2$, and is completely analogous to figure 4 of [51]. Notice that the results for $\theta_0 = \pi/2$ and $\theta_0 = \pi/3$ are very similar. Each curves corresponds to a fixed radial quantum number n. For $\theta_0 = \pi/2$ and $\theta_0 = \pi/3$ and $n = 1, 2$ and 3 the Shannon entropy increases with the angular momentum quantum number m until it reaches a maximum value, to then decrease in the region $0 < m < 5$. States with $n > 3$ reach a maximum for $m > 5$. The shift of the position of the maximum becomes more evident as the angular aperture of the cone is dereceased as shown for $\theta_0 = \pi/9$ and $\theta_0 = \pi/18$.

In all the graphs in figure 7, the Shannon entropy S_r decreases as angular momentum m increases. Corzo *et al* [51] gave the explanation of this behavior for $\theta_0 = \pi/2$. The explanation for the other angles θ_0 follows immediately by looking at figures 5 and 6.

5.2. Momentum space

In figure 8 we show the Shannon entropy in momentum space S_p as a function of the confining radius for the following values of the apex angle $\theta_0 = \pi/2,\ \pi/3,\ \pi/9$.

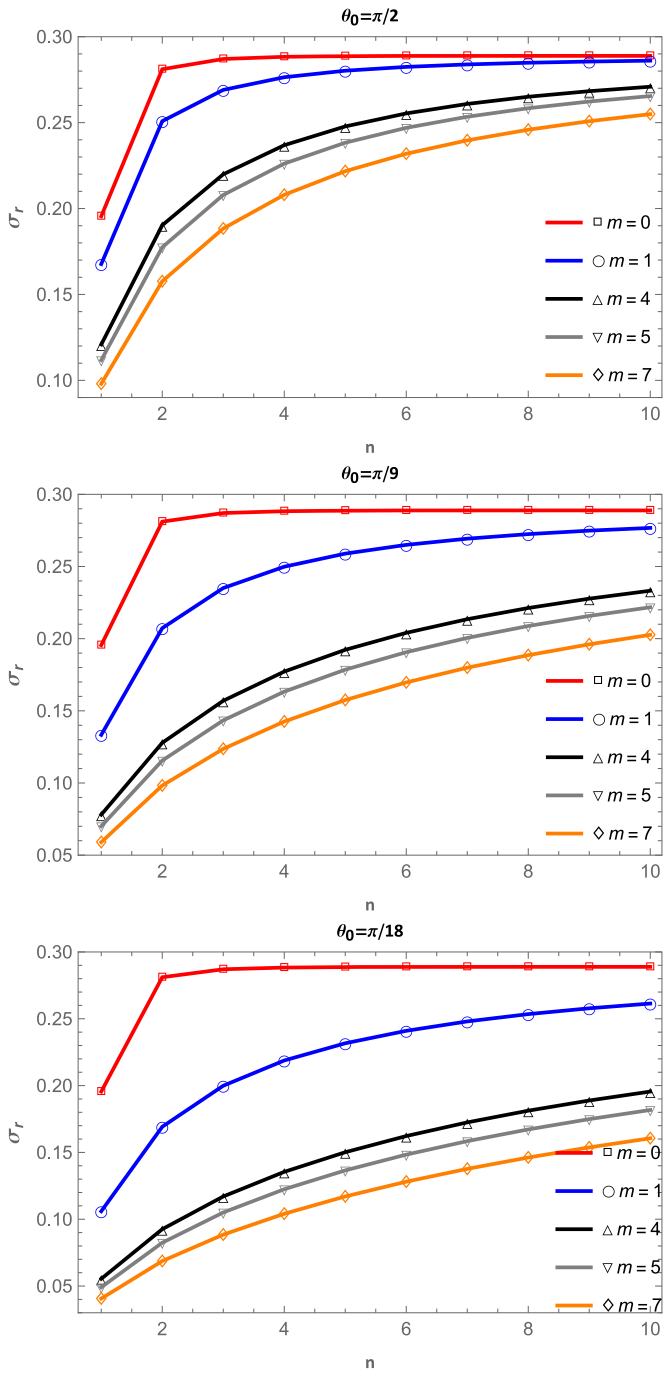

Figure 12. Radial standard deviation as a function of the radial quantum number n for three different apex angles $\theta_0 = \pi/2,\ \pi/9$ and $\pi/18$ and for a value of $r_0 = 1$.

As r_0 diminish the Shannon entropy grows (delocalization) for all the states. The S_p curves for $\theta_0 = \pi/2$ and $\theta_0 = \pi/3$ are very similar. For a fixed value of r_0 the value of S_p increases (delocalization) as the apex angle diminishes, for any state. The Shannon entropy S_p curves for the states (1, 1) and (2, 0) approach as θ_0 decreases.

In figure 9 we show the behavior of the Shannon entropy S_p as a function of the radial quantum number n for $r_0 = 1$.

The Shannon entropy S_p diminishes (localization) as n decreases, two groups of states are formed, one for states $m = 0$ and 1 and the other for states with $m = 4$ –7, for a fixed value of n the Shannon entropy S_p increases with m. The separation between the S_p curves, for the states with $m = 0$ and 1, becomes more evident as the angle θ_0 decreases.

In figure 10 we show the Shannon entropy S_p as a function of m for $\theta_0 = \pi/2,\ \pi/3,\ \pi/9$ and $\pi/18$. Shannon entropy S_p grows (delocalization) as m increases.

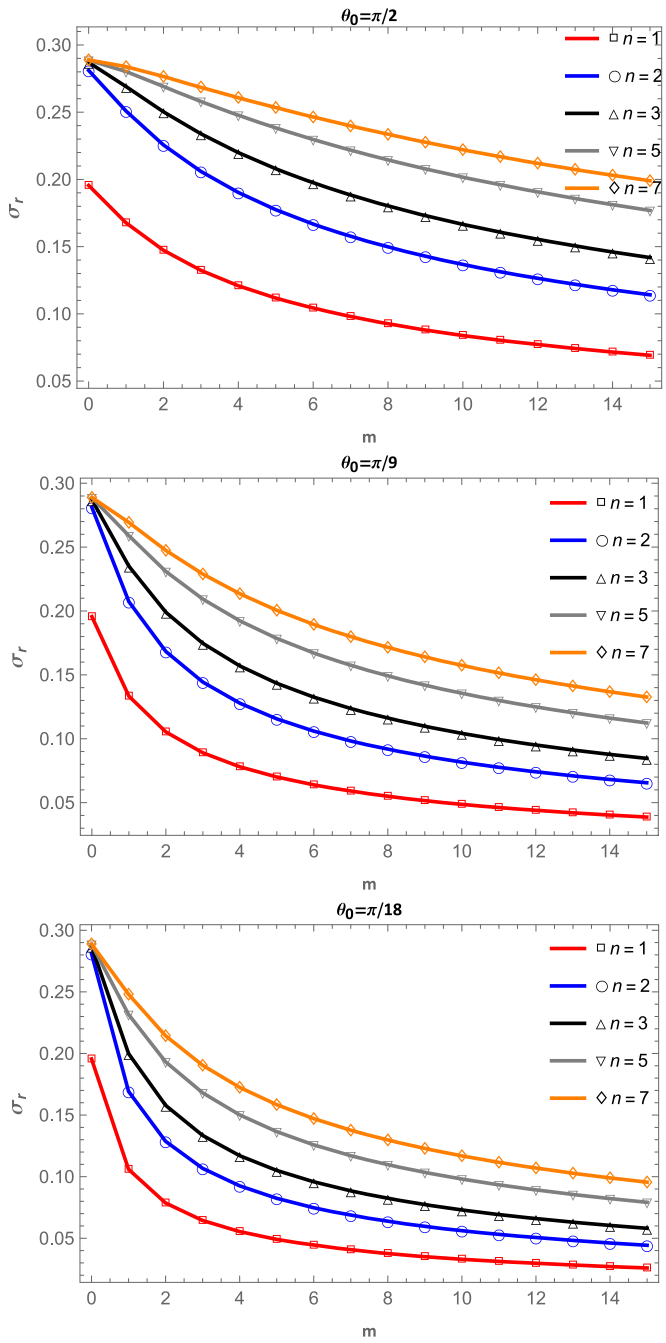

Figure 13. Radial standard deviation as a function of the angular quantum number m for three different apex angles $\theta_0 = \pi/2,\ \pi/9$ *and* $\pi/18$ and for a value of $r_0 = 1$.

5.3. Shannon entropic sum

The BBM uncertainty principle equation (28) for the present two-dimensional ($D = 2$) problem is reduced to

$$S_t = S_r + S_p \geqslant 2(1 + \ln \pi) = 4.2896. \tag{31}$$

In figures 11(a) and (b), we show the Shannon entropy in configuration and momentum spaces and the total Shannon entropy, the BBM uncertainty principle [63] is satisfied in all cases and the value of the total entropy remains constant. It should be noted that the position of the crossings between Shannon entropy S_r and S_p increases as the apex angle θ_0 decreases. It is also interesting to note that the S_r and S_p curves are symmetrical with respect to each other.

5.4. The radial standard deviation

In figure 12 we show the radial standard deviation as a function of the radial quantum number n for different values of the angular momentum m, for $\theta_0 = \pi/2,\ \pi/9$ and $\pi/18$. The curves corresponding to $\theta_0 = \pi/2$ are in complete agreement with figure 2 of [51]. The curve of σ_r corresponding to $m = 0$ grows (delocalization) with n and reaches its asymptotic value quickly for the three angles. The curves of σ_r for $m = 1,\ldots,7$ also grow (delocalization) as a function of n, for the three studied angles. This behavior does not agree with what was found in section 5.1, in which it was found that the states $(n, 0)$ and $(n, 1)$ are more localized as n increases (figure 4).

In figure 13 we show the behavior of the radial standard deviation σ_r as a function of m for different values of n. σ_r diminished (localization) as m grows, for the three studied angles. This behavior is also inconsistent with what was found in section 5.1, in which it was found that the Shannon entropy curves as a function of m first increase and reach a maximum value (delocalization) and then decrease (localization), as can be seen in figure 7.

6. Conclusions

In this work we use curvilinear coordinates $(r,\ \phi)$ to obtain the Schrödinger equation for an electron on the cone surface, we found the exact energies and wave functions for all states. We also studied the Shannon entropies in configuration and momentum space, and the entropic sum, as a function of the confinement radius r_0 and the apex angle θ_0.

The Shannon entropy for the case $\theta_0 = \pi/2$ is reduced to that of a particle inside a circular box of radius r_0, the results found in this work are in full agreement with those previously published [51–53].

The Shannon entropy in configuration space, for all states, decreases (localization) as the confining radius r_0 decreases. This behavior can be explained by the fact that as the confinement radius r_0 decreases, the surface on which the electron moves also decreases, and therefore the electron is more localized. On the other hand, as r_0 decreases the value of the Shannon entropy in the momentum space S_p increases, so that the BBM uncertainty relation (equation (28)) is satisfied for all states and for all values of the apex angle θ_0.

The for a fixed value of r_0 the Shannon entropy diminishes as the apex angle θ_0 decreases, this decrease in S_r is most evident for small angles. When the spatial confinement increases, the area in which the electron moves is reduced, the Shannon entropy decreases (localization) and even its value can become negative, this is a typical behavior of the Shannon entropy in confined systems [46–57]. In the momentum space the opposite happens, for a fixed r_0, the Shannon entropy S_p increases as the apex angle decreases.

The behavior of the Shannon entropy in configuration space as a function of the quantum number n depends on the state (n, m). The S_r curve for states $(n, 0)$ for the apex angle $\theta_0 = \pi/2,\ \pi/3,\ \pi/9$ and $\pi/18$, are decreasing functions of n. S_r for the states $(n, 1)$ is a decreasing function of n for the angles $\theta_0 = \pi/2,\ \pi/3,\ \pi/9$ and for $\pi/18$ has a maximum. For other higher excited states, the entropy increases, reach a maximum and then diminish as a function of n for $\theta_0 = \pi/2,\ \pi/3$, for smaller values of θ_0 the S_r curves are increasing function of n, as can see from figure 4. Whereas in momentum space, the curves of S_p are increasing functions of n for all studied states (n, m) and for $\theta_0 = \pi/2,\ \pi/3,\ \pi/9$ and $\pi/18$.

The behavior of Shannon entropy in configuration space as a function of the quantum number m depends on the state (n, m). The S_r curves as a function of m ha a maximum for states (n, m), and for $\theta_0 = \pi/2,\ \pi/3,\ \pi/9$ and $\pi/18$. As the apex angle θ_0 diminishes the position of the maximum of each curve move toward the maximun of the curve for $m = 1$ (figure 7). The behavior of Shannon entropy in momentum space S_p is simpler, they are increasing functions of m for all studied states for $\theta_0 = \pi/2,\ \pi/3,\ \pi/9$ and $\pi/18$.

We computed the radial standar deviation as a function of the quantum number n for different values of angular momentum m, for $\theta_0 = \pi/2,\ \pi/3$, and $\pi/18$ (figure 12). We find that the radial standard deviation predicts different behavior to the Shannon entropy.

We also computed the radial estandar deviation as a function of the angular momentum m for different values of the radial quantum number, for $\theta_0 = \pi/2,\ \pi/3$, and $\pi/18$ (figure 13). The radial estandar deviation show localization as the quantum number m increases. However, Shannon entropy (figure 7) shows first a delocalization, and as m increases, a localization, this behavior is in agreement with the probability distribution plots in figures 5 and 6.

The Shannon entropy is more appropriate than the radial standard deviation to describe the localization-delocalization of a particle moving on the surface of a cone.

Acknowledgments

(LMA) would like to thank the CONAHCYT (Mexico) and the Metropolitan Autonomous University–Iztapalapa (UAM-I) for their continued support.

Data availability statement

Including the data supporting this research would make the size of the manuscript excessively large. The data that support the findings of this study are available upon reasonable request from the authors.

ORCID iDs

N Aquino https://orcid.org/0000-0002-3795-0304

References

[1] Fernández F M and Castro E A 1982 *Kinam* **4** 193–223
[2] Fröman P O, Yngve S and Fröman N J 1987 *J. Math. Phys.* **28** 1813
[3] Yngve S J 1988 *J. Math. Phys.* **29** 931
[4] Jaskólski W 1996 *Phys. Rep.* **271** 1
[5] Buchachenko A L 2001 *J. Phys. Chem.* **105** 5839
[6] Connerade J P, Dolmatov V H and Lakshmi P A 2000 *J. Phys. B: At. Mol. Opt. Phys.* **33** 251
[7] Sabin J R, Brändas E and Cruz S A (ed) 2009 *Adv. Quantum Chem.* 58 (Academic)
[8] Sen K D (ed) 2014 *Electronic Structure of Quantum Confined Atoms and Molecules* (Springer)
[9] Bányai L and Koch S W 1993 *Semiconductor Quantum Dots* (World Scientific)
[10] Michels A, de Boer J and Bijl A 1937 *Physica* **4** 981–94
[11] Ley-Koo E and Rubinstein S 1979 *J. Chem. Phys.* **71** 351
[12] Montgomery H E Jr and Sen K D 2012 *Phys. Lett.* A **376** 1992–6
[13] Frapiccini A L and Mitnik D M 2021 Study of hydrogen confined in onion shells *Eur. Phys. J.* D **75** 41
[14] Aquino N, Granados V and Yee-Madeira H *Rev. Méx. Fís.* **55** 125–9 (200)
de Oliveira Batael H, Filho E D, Chahine J and da Silva J F 2021 Efects of quantum confinement on thermodynamic properties *Eur. Phys. J.* D **75** 52
[15] Jha R, Giri S and Chattaraj P K 2021 Does confinement alter the ionization energy and electron affinity of atoms? *Eur. Phys. J.* D **75** 88
[16] Wigner E P and Huntington H B 1935 *J. Chem. Phys.* **3** 764
[17] Sen K D, Pupyshev V I and Montgomery H E 2009 *Adv. Quantum Chem.* (Elsevier) pp 25–77
[18] Sil A N, Canuto S and Mukherjee P K 2009 *Adv. Quantum Chem.* (Elsevier) pp 115–75
[19] Ley-Koo E 2018 *Rev. Mex. Fís.* **64** 326–63
[20] Schmidbauer M, Seydmohamadi S and Grigoriev D 2006 *Phys. Rev. Lett.* **96** 066108
[21] Lu M, Yang X J, Perry S S and Rabalais J W 2002 *Appl. Phys. Lett.* **80** 2096
[22] Mohammadi S A, Khordad R and Rezaei G 2016 *Physica* E **76** 203
[23] Khordad R and Bahramiyan H 2015 *Physica* E **66** 107
[24] Ledentsov N N, Ustinov V M, Shchukin V A, Kopev P S, Alferov Z I and Bimberg D 1998 *Semiconductors* **32** 343
[25] Khordad R and Bahramiyan H 2014 *Eur. Phys. J. Appl. Phys.* **67** 20402
[26] Dhingra M, Shankar A and Tiwari B B 2010 *Indian J. Phys.* **84** 1031
[27] Bimberg D, Grudmann M and Ledentsov N N 1999 *Quantum Dot Hetrostructures* (Wiley)
[28] Dosi A A 2018 Quantum cones and quantum balls, *Azerb. J. Math.* **8** 142–51 (https://azjm.org/volumes/0802/0802-9.pdf)
[29] 't Hooft G 1988 *Commun. Math. Phys.* **117** 685
Deser S and Jackiw R 1988 *ibid* **118** 495
Gerbert P S and Jackiw R 1989 *ibid.* **124** 229
[30] Lancaster D 1990 *Phys. Rev.*D **42** 2678
[31] Gravesen J, Willatzen M and Lew-Yan-Voom L C 2005 Quantum-mechanical particle confined to surface of revolution-truncated cone and elliptic torus case studies *Phys. Scr.* **72** 105–11
[32] Saraiva P 2023 On Shannon entropy and its aplications *Kuwai Journal of Science* **50** 194–9
[33] Frieden B R 1998 *Physics from Fisher Information: A Unification* (Cambridge University Press)
[34] Rivastava A 2002 Stocastic models for capturing image variability *IEEE Signal Process Mag.* **19** 63–76
[35] Huang J, Supaongprapa T, Terakura I, Wang F, Ohnishi N and Sugie N 1999 A model-based sound localization system and its application to robot navigation *Rob. Aut. Syst.* **27** 199–209
[36] Prato M and Zanni N 2008 Inverse problem in machine learning: an application to brain activity interpretation *J. Phys. Conf. Ser.* **135** 012085
[37] Wang Y 2016 *Seismic Inversion: Theory and Applications* (Wiley Blackwell)
[38] Grasshans F and Cerf N J 2004 Continuous-variable quantum cryptography is secure against non-gaussian attacks *Phys. Rev. Lett.* **92** 047905
[39] Wyner A D and Shamai S 1998 Information-theoretic considerations for symmetric, cellular, multiple-access fading channels—part I *Proc. IEEE* **86** 442
[40] Casadio R, da Rocha R, Meert P, Tabarroni L and Barreto W 2023 Configurational entropy of black hole quantum cores *Class. Quantum Grav.* **40** 075014
[41] Dehesa J S, Belega E D, Toranzo I V and Apterakev A I 2019 The Shannon entropy of high-dimensional hydrogenic and harmonic systems *Int. J. Quantum Chem.* **119** e25977
[42] Bouvrie P A, Angulo J C and Dehesa J S 2011 Entropy and complexity analysis of Dirac-delta-like quantum potentials *Phys.* A **390** 2215
[43] Sun G H, Aoki M A and Dong S H 2013 Quantum information entropies of the eigenstates for the Pöschl—Teller-like potential *Chin. Phys.* B **22** 050302
[44] Joshi R, Verma N and Mohan M 2023 Shannon entropy along hydrogen isoelectric sequence using numerov method *Rev. Méx. Fís.* **69** 060401
[45] Savirov D and Koledina K 2020 Classification of isentropic molecules in terms of Shannon entropy *EPJ Web of Conferences* **244** 01016
[46] Sen K D 2005 *J. Chem. Phys.* **123** 074110

[47] Aquino N, Flores-Riveros A and Rivas-Silva J F 2013 *Phys. Lett.*A **377** 2062–8
[48] Rodríguez-Bautista M, Vargas R, Aquino N and Garza J 2017 *Int. J. Quantum Chem.* **118** 25571
[49] Estañón C R, Aquino N, Puertas-Centeno D and Dehesa J S 2020 *Int. J. Quantum Chem.* **120** e26192
[50] Nascimento W S and Prudente F V 2016 *Quim. Nova* **39** 757–64
[51] Corzo H H, Castaño E, Laguna H G and Sagar R P 2013 Measuring localizatio-delocalization phenomena in a quantum corral *J. Math. Chem.* **51** 179–93
[52] Song X D, Sun G H and Dong S H 2015 Shannon information entropy for an infinite circular well *Phys. Lett.* A. **379** 1402–8
[53] Cruz E 2023 Doctoral Tesis, Effects of electric and magnetic fields on some confined quantum systems of a one electron. Universidad Autónoma Metropolitana-Iztapalapa, Mexico City, Mexico. (https://doi.org/10.24275/uami.ng451h973)
[54] Estañón C R, Montgomery H E, Angulo J C and Aquino N 2024 The confined helium atom: An informational-theoretic approach *Int. J. Quantum Chem.* **124** e27358
[55] Majumdar S and Roy A K 2020 Shannon entropy in confined helium-like ions within a Density Functional formalism *Quantum Rep.* **2** 189–207
[56] Nasser I, Zeama M and Abdel-Hady A 2020 Rényi, Fisher, Shannon and their electron correlation tools for two-electron series *Phys. Scr.* **95** 095401
[57] Martínez-Flores C 2021 Shannon entropy and Fisher information for endohedral one an two-electron atoms *Phys. Lett.* A **386** 126988
[58] Coomar A, Jones K and Adamowicz L 2022 Quantum states of a confined hydrogen atom calculated in a basis of explicitly correlated Gaussians *Chem. Phys. Lett.* **790** 139358
[59] Lima F C C, Moreira A R P, Almeida C A S, Edet C O and Ali N 2023 Quantum information entropy of a particle trapped by the Aharonov–Bohm-type effect *Phys. Scr.* **98** 065111
[60] Wrede R C 1972 *Introduction to Vector and Tensor Analysis* (Dover Publications, Inc) ch 3
[61] Greiner W and Bromley D A 1989 *Quantum Mechanics an Introduction* (Springer) ch 8 p 194
[62] NIST Digital Library of Mathematical Functions (https://dlmf.nist.gov/)
[63] Bialinicki-Birula I and Mycielski J 1975 *Comm. Math. Phys.* **44** 129